V European Conference on Computational Fluid Dynamics
ECCOMAS CFD 2010
J. C. F. Pereira and A. Sequeira (Eds)
Lisbon, Portugal, 14–17 June 2010

NUMERICAL SIMULATION OF BLOOD FLOWS IN A VESSEL WITH VALVES BASED ON VIRTUAL-FLUX METHODS

T. FUKUI[*] and K. MORINISHI[†]

[*]Dept. of Mech. and Syst. Eng., Kyoto Inst. Tech.
Goshokaido-cho, Matsugasaki, Sakyo-ku, Kyoto 606-8585, Japan
e-mail: fukui@kit.ac.jp

[†]Dept. of Mech. and Syst. Eng., Kyoto Inst. Tech.
Goshokaido-cho, Matsugasaki, Sakyo-ku, Kyoto 606-8585, Japan
e-mail: morinisi@kit.ac.jp

Key words: Aortic Valve, Aortic Stenosis, Blood Flows, Virtual-Flux Methods

Abstract. *Aortic valve is a membrane that plays an important role in controlling effective outputs of blood flow from the heart. Aortic stenosis is a disease that aortic valves barely open in systole, which cause considerable reduction of amount of blood flow. In this study, we performed numerical simulation of blood flows in a parallel-plate channel with valves. Lattice Boltzmann method for 2-dimentional 9-velocity (D2Q9) model is used as a governing equation, and virtual-flux methods are applied to express thin valves in a flow. The channel length L is 10 times as long as the distance between the parallel-plate D with a grid number of 2002 × 202 on a regular Cartesian coordinate system. The valves whose length is D/2 are placed at P_v = 2D from the inlet. The length of the valve hinge h is D/20. The angle of the down valve θ_d is set to 0 to $4\pi/18$ at the interval of $0.5\pi/18$, and that of the upper valve θ_u is determined according to the opening area of the valve S. The flow fields strongly depend on the valve angle. Steady flow can be observed from the down valve angle θ_d of $1.5\pi/18$ to $2.5\pi/18$, and the pressure coefficient C_p is relatively low in this range. The pressure coefficient C_p is higher when the valve angle θ_d or θ_u is near 0.*

1 INTRODUCTION

The aortic valve consists of three thin membranous cusps, which in the open position are displaced outward toward the aorta to eject blood in the left ventricle, and come together to seal the aortic orifice in the closed position [1]. The heart pumps blood throughout the body efficiently owing to the heart valves operation. Aortic stenosis (AS) is one of the most common diseases related to dysfunction of the heart valves. The opening area of the valve decreases due to AS, which cause considerable reduction of amount of blood flow. Congenitally, 1% to 2% of the population is born with a bicuspid aortic valve, and frequently evolves into stenosis [2]. A higher percentage of congenital bicuspid aortic valves develop left ventricular (LV) outflow obstruction [3]. LV

pressure overload with AS causes increased LV wall thickness to maintain normal and transmural wall stress [4].

Clinically, the severity of AS is evaluated by estimating the opening area of the valve. The opening area determined by using planimetry to trace manually at the level of the orifice usually includes some errors [5]. The error of measurement using this method is potentially significant for calcific AS, as the computer assumes a circle for area calculation. Pressure gradients across the stenotic valve may be another index for evaluation of the degree of AS, and measured using the echocardiographic velocity or by direct pressure measurements during cardiac catheterization. A modification of the Bernoulli equation is applied to determine the pressure gradient [2], however, there is a tendency for pressure gradients derived by echo data to be larger than those directly measured using invasive cardiac catheters. It is necessary to know blood flows around aortic valve and pressure drop changes due to AS in advance. Numerical simulation is expected to lead to a better understanding of AS and its dependence on flow parameters.

The method of lattice Boltzmann equation (LBE) is a simple kinetic-based approach for fluid flow computation. The LBE has advantages its simple coding and its locality, which makes it intrinsically parallelizable [6], and has been applied to many general problems [7,8,9], and those relevant to blood flow simulation [10,11,12], as well. Especially, Krafczyk et al. [13] studied 3D transient blood flows around artificial aortic valve by lattice Boltzmann methods. They, however, simplified the problem by assuming the valve leaflets as being fixed. In this study, we apply the virtual flux method (VFM) [14], which is a tool to describe stationary or moving body shapes, to the 2D aortic valve, and consider the blood flow fields.

2 METHODS

2.1 Governing equation

The discrete velocity Boltzmann equation (DVBE) is as follows,

$$\frac{\partial f_\alpha}{\partial t} + \boldsymbol{e}_\alpha \cdot \nabla f_\alpha = \boldsymbol{\Omega}_\alpha, \tag{1}$$

where $\boldsymbol{e}_\alpha$ is the discrete particle velocity, f_α is the distribution function associated with $\boldsymbol{e}_\alpha$, and Ω_α is the collision operator. The collision operator, which is very complicated, is usually approximated by the simple single-relaxation-time Bhatnagar-Gross-Krook (BGK) model [15]:

$$\boldsymbol{\Omega}_\alpha = -\frac{1}{\tau}\left(f_\alpha - f_\alpha^{(eq)} \right), \tag{2}$$

where $f_\alpha^{(eq)}$ is the equilibrium distribution function, and τ is the relaxation time. The evolution of the distribution function f_α for the lattice Boltzmann equation (LBE) can be written as

$$f_\alpha\left(\boldsymbol{x} + \boldsymbol{e}_\alpha \Delta t, t + \Delta t\right) - f_\alpha\left(\boldsymbol{x}, t\right) = -\frac{1}{\tau}\left\{ f_\alpha\left(\boldsymbol{x}, t\right) - f_\alpha^{(eq)}\left(\boldsymbol{x}, t\right) \right\}. \tag{3}$$

In this study, we use a 2D square lattice model with 9 velocities, which is referred to as the D2Q9 model. The particle distribution of the D2Q9 model is shown in Fig. 1. There exist three different speeds according to its direction, i.e.,

$$\left|\boldsymbol{e}_\alpha\right| = 0 \ (\alpha = 0),$$

$$\left|\boldsymbol{e}_\alpha\right| = c \ (\alpha = 1,\ 2,\ 3,\ 4), \qquad (4)$$
$$\left|\boldsymbol{e}_\alpha\right| = \sqrt{2}c \ (\alpha = 5,\ 6,\ 7,\ 8),$$

where $c = \delta x / \delta t$, δx and δt are the lattice constant and the time step size, respectively. At each time step, particles propagate along the lattice link to the next neighbors.

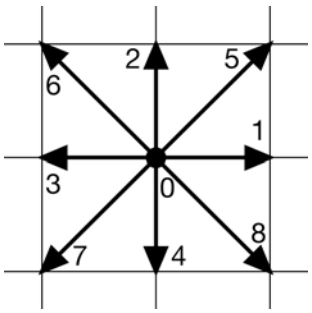

Figure 1: Particle distribution of the D2Q9 model

It is shown that the Navier-Stokes equations can be derived from the LBE though a Chapman-Enskog expansion procedure in the incompressible limit [16] with a relaxation time τ as

$$\tau = \frac{3\nu}{c\delta x} + \frac{\delta t}{2}. \qquad (5)$$

The most common choice for the equilibrium distribution function $f_\alpha^{(eq)}$ is the truncated form of the Maxwell distribution, which is a very good approximation for small Mach numbers [17].

$$f_\alpha^{(eq)} = \omega_\alpha \rho \left[1 + \frac{3\left(\boldsymbol{e}_a \cdot \boldsymbol{u}\right)}{c^2} + \frac{9\left(\boldsymbol{e}_\alpha \cdot \boldsymbol{u}\right)^2}{2c^4} - \frac{3\boldsymbol{u}^2}{2c^2}\right], \qquad (6)$$

where ω_α is the weight coefficients given as follows,

$$\omega_\alpha = 4/9 \ (\alpha = 0),$$
$$\omega_\alpha = 1/9 \ (\alpha = 1,\ 2,\ 3,\ 4), \qquad (7)$$
$$\omega_\alpha = 1/36 \ (\alpha = 5,\ 6,\ 7,\ 8).$$

Macroscopic quantities such as density ρ and momentum $\rho\boldsymbol{u}$ can be directory evaluated as

$$\rho = \sum_\alpha f_\alpha, \qquad (8)$$
$$\rho\boldsymbol{u} = \sum_\alpha f_\alpha \boldsymbol{e}_\alpha. \qquad (9)$$

In this paper, we choose the incompressible D2Q9 model proposed by He and Luo [18]. The distribution function p_α, equilibrium distribution function $p_\alpha^{(eq)}$, and macroscopic quantities for incompressible model are given as follows,

$$p_\alpha = c_s^2 f_\alpha, \qquad (10)$$

$$p_\alpha(\boldsymbol{x}+\boldsymbol{e}_\alpha\Delta t, t+\Delta t) - p_\alpha(\boldsymbol{x},t) = -\frac{1}{\tau}\left\{ p_\alpha(\boldsymbol{x},t) - p_\alpha^{(eq)}(\boldsymbol{x},t)\right\}, \tag{11}$$

$$p_\alpha^{(eq)} = \omega_\alpha\left[p + \rho_0\left(\left(\boldsymbol{e}_\alpha\cdot\boldsymbol{u}\right) + \frac{3}{2}\frac{\left(\boldsymbol{e}_\alpha\cdot\boldsymbol{u}\right)^2}{c^2} - \frac{1}{2}\boldsymbol{u}^2 \right)\right], \tag{12}$$

$$p = \sum_\alpha p_\alpha\,, \tag{13}$$

$$\boldsymbol{u} = \frac{1}{\rho_0 c_s^2}\sum_\alpha p_\alpha \boldsymbol{e}_\alpha\,, \tag{14}$$

where c_s is the sound speed and ρ_0 is the initial density. The initial density ρ_0 is set to 1.0, and the sound speed c_s is given by

$$c_s = \frac{c}{\sqrt{3}}. \tag{15}$$

2.2 Boundary conditions

Boundary conditions are taken to expand the distribution function. Figure 2 shows an example of cell vertex boundary. The distribution function p_α at the boundary point b is given by

$$p_{\alpha,\mathrm{b}} = p_\alpha^{(eq)}\left(\boldsymbol{u}_\mathrm{b}, p_\mathrm{b}\right) + \left(p_{\alpha,1} - p_{\alpha,1}^{(eq)}\right), \tag{16}$$

where $p_\alpha{}^{(eq)}(\boldsymbol{u}_\mathrm{b},\ p_\mathrm{b})$ is the equilibrium distribution function, whose macroscopic quantities $\boldsymbol{u}_\mathrm{b}$ and p_b satisfy the boundary condition. In case of no-slip condition on the boundary, for instance, zero pressure gradient (Eq. (17)) and zero velocity (Eq. (18)) are assumed for estimating the macroscopic quantities on the boundary.

$$p_\mathrm{b} = \frac{4p_1 - p_2}{3}, \tag{17}$$

$$\boldsymbol{u}_\mathrm{b} = \boldsymbol{0}, \tag{18}$$

where p_1 and p_2 are the pressure at the neighboring points 1 and 2, respectively.

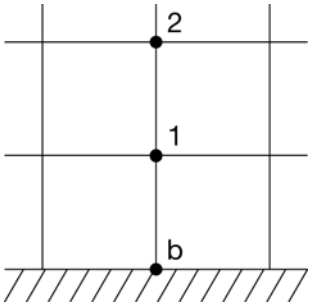

Figure 2: Cell vertex boundary

The virtual flux method (VFM) enables us to estimate flow field around arbitrary body shapes properly in a Cartesian grid [14]. In this study, we apply the VFM to express arbitrary body shapes appropriately in case that boundary points are not located

on the cell vertex. Figure 3 shows an example of virtual flux boundary, where the virtual boundary point b is placed between cell vertexes 1 and 3. When the distribution function at vertex 1 is obtained, the distribution function at vertex 3, which includes the effect of the virtual boundary, is necessary, and vice versa. The macroscopic quantities on the virtual boundary point b are then determined to satisfy the boundary conditions. No-slip condition on the boundary, for example, is attained to assume zero pressure gradient (Eq. (19)) and zero velocity (Eq. (20)) on the boundary.

$$p_b = \frac{\left(1+r\right)^2 p_1 - r^2 p_2}{\left(1+r\right)^2 - r^2}, \tag{19}$$

$$\boldsymbol{u}_\mathrm{b} = \mathbf{0}, \tag{20}$$

where r is the distance between vertex 1 and virtual boundary point b. Next, the equilibrium distribution function $p_\alpha^{(eq)}$ and distribution function p_α at the virtual boundary point b are obtained through Eqs. (12) and (16). The distribution function p_α at the vertex 3 is then estimated to extrapolate that at the virtual boundary point b.

$$p_{\alpha,3} = \frac{p_{\alpha,\mathrm{b}} - \left(1-r\right)p_{\alpha,1}}{r}. \tag{21}$$

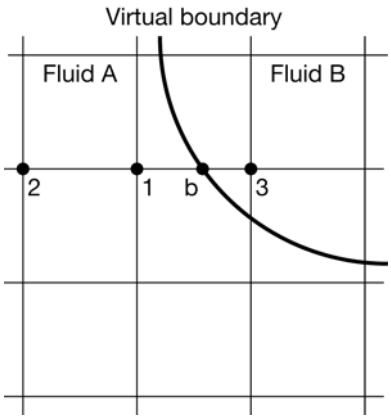

Figure 3: Virtual flux boundary

2.3 Computational model

Numerical simulation of blood flow in a parallel-plate channel with valves is performed. Figure 4 shows the schematic view of the simulation model used in this study. The channel length L is 10 times as long as the distance between the parallel-plate D with a grid number of 2002 × 202 on a regular Cartesian coordinate system. The valves whose length is $D/2$ are placed at $P_v = 2D$ from the inlet. The length of the valve hinge h is $D/20$. The angle of the down valve θ_d is set to 0 to $4\pi/18$ at the interval of $0.5\pi/18$, and that of the upper valve θ_u is determined according to the opening area of the valve S, which is assumed to be constant and is set to 0.60 in this analysis. The relationships among these parameters are consequently as follows,

$$S = D - \left\{ \left(\frac{D}{2} - h \right) \left(\sin\theta_d + \sin\theta_u \right) + 2h \right\} = \text{constant}. \tag{22}$$

The boundary conditions are that $\boldsymbol{u} = (u_0, 0)$ and p is linearly extrapolated at the inlet, $p = p_0$ and $\boldsymbol{u}$ is linearly extrapolated at the outlet, and no-slip on the wall and the valves. The parameters are that $u_0 = 0.1c$, and $p_0 = 1/3$. The Reynolds number Re is set to 400.

The pressure coefficient C_p is defined as below, and used to evaluate the pressure change related to the valve angles.

$$C_p = \frac{p - p_0}{\frac{1}{2}\rho_0 u_0^2}. \tag{23}$$

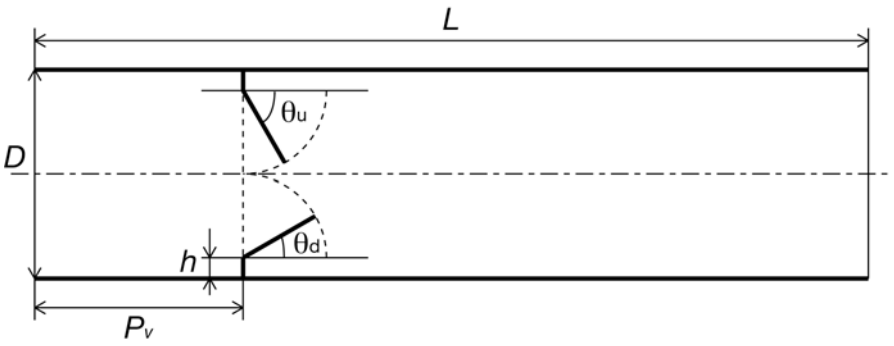

Figure 4: Schematic view of the parallel-plate channel with valves

3 RESULTS AND DISCUSSION

The flow fields strongly depend on the valve angle. Figures 5 show the pressure contours and axial velocity distribution in a parallel-plate channel with the down valve angle θ_d of $2\pi/18$. The corresponding upper valve angle θ_u is $1.89\pi/18$. The pressure and axial velocity are steady in time, and those of the proximal region to the valve ($0 < x < P_v$) are nearly axisymmetric. The space-averaged pressure coefficient C_p of this region is 1.47. Figures 6 show the pressure contours and axial velocity distribution with the down valve angle θ_d of $4\pi/18$ at the non-dimensional time interval of 1/100. The corresponding upper valve angle θ_u is $0.14\pi/18$. The lower pressure region spreads mainly behind the down valve, which consequently oscillates the high axial velocity region downstream near the outlet. The space-averaged pressure coefficient C_p of the proximal region to the valve is 1.82 to 2.09 in a cycle, and time variation of the C_p is shown in Fig. 7. The non-dimensional period T of the C_p is about 0.11. Figure 8 shows the relationships between pressure coefficient C_p and down valve angle θ_d. The time-averaged value of the pressure coefficient C_p in a cycle is represented with a circle. If the flow is unsteady, the maximum and minimum values are indicated with bars. Steady flow can be observed from the down valve angle θ_d of $1.5\pi/18$ to $2.5\pi/18$, and the pressure coefficient C_p is relatively low in this range. The pressure coefficient C_p is higher when the valve angle θ_d or θ_u is near 0. The time variation range of the pressure coefficient C_p with the down valve angle θ_d of 0 is large enough to enclose that with the down valve angle θ_d of $0.5\pi/18$.

In future work, we apply the VFM to the moving valve, which is caused by hemodynamic forces, to reproduce more realistic aortic valve behavior, and flow pattern analyses are necessary to consider the severity of AS.

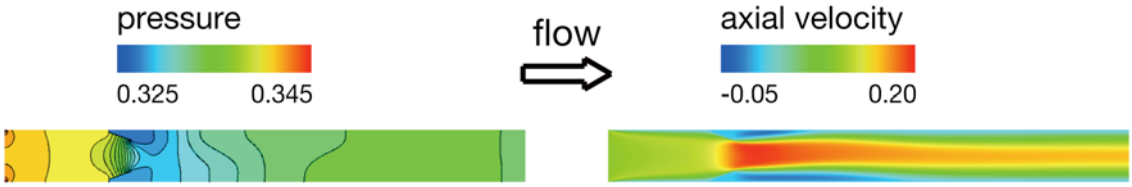

Figure 5: Pressure contours and axial velocity distribution in a parallel-plate channel with the down valve angle θ_d of 2π/18

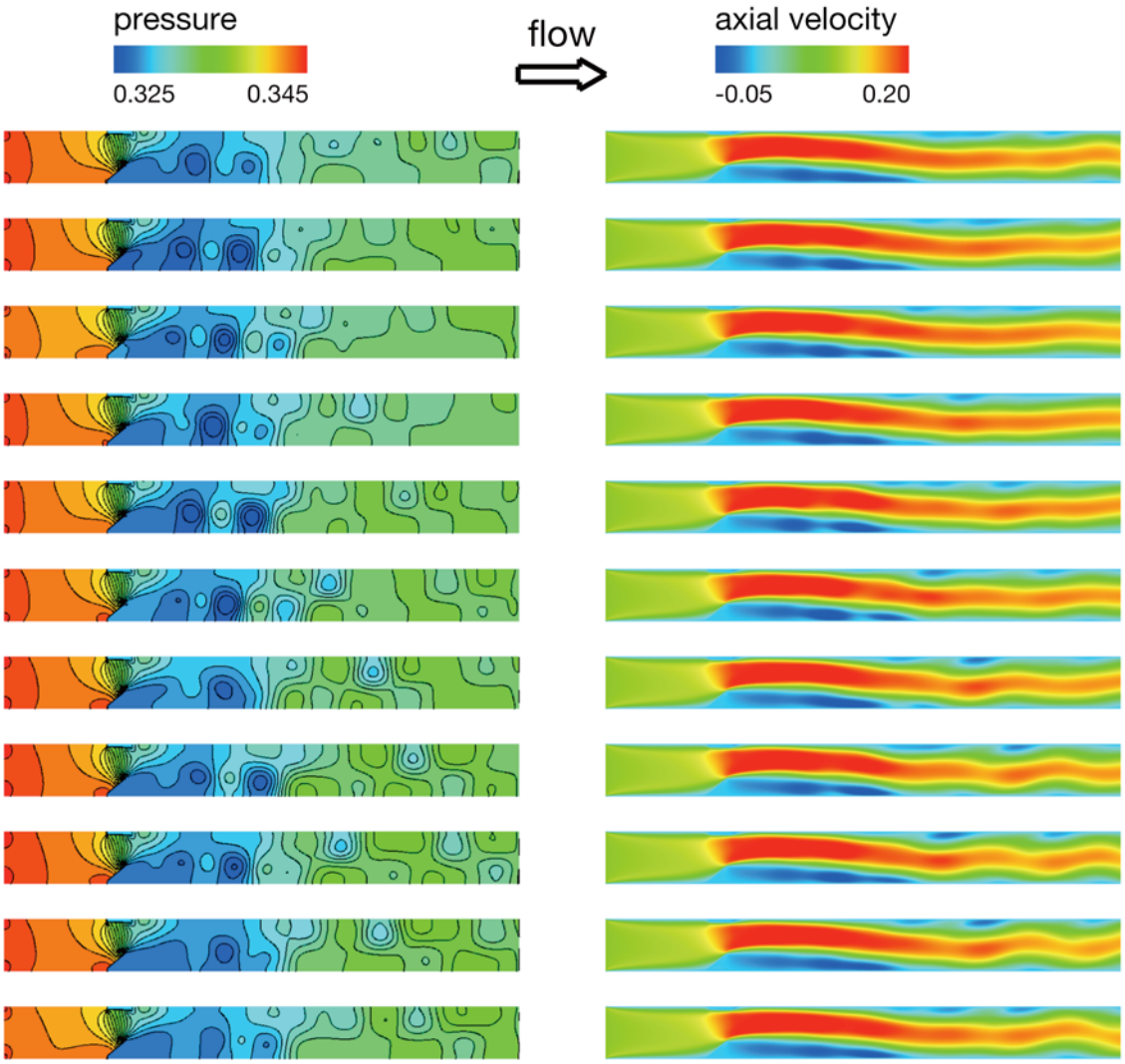

Figure 6: Pressure contours and axial velocity distribution with the down valve angle θ_d of 4π/18 at the non-dimensional time interval of 1/100

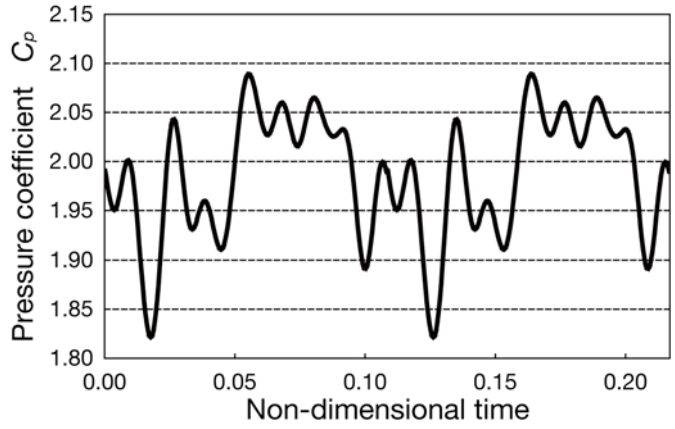

Figure 7: Pressure coefficient C_p diagram of the model with the down valve angle θ_d of 4π/18

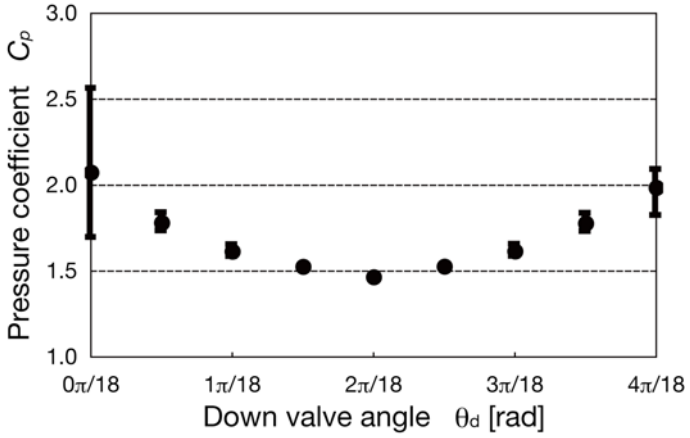

Figure 8: Relationships between pressure coefficient C_p and down valve angle θ_d

REFERENCES

[1] Y.C. Fung, Biomechanics: circulation, 2nd Edition, *Springer*, (1997).

[2] B.A. Carabello, Aortic stenosis, *N. Engl. J. Med.*, **346**(9), 677-682 (2002).

[3] C.Z. Zigelman and P.M. Edelstein, Aortic valve stenosis, *Anesthesiol. Clin.*, **27**(3), 519-532 (2009).

[4] W. Grossman, D. Jones, and L.P. McLaurin, Wall stress and patterns of hypertrophy in the human left ventricle, *J. Clin. Invest.*, **56**, 56-64 (1975).

[5] A.D. Friedrich and P.S. Shekar, Interrogation of the aortic valve, *Crit. Care Med.*, **35**(8 Suppl), S365-S371 (2007).

[6] T. Kruger, F. Varnik, and D. Raabe, Shear stress in lattice Boltzmann simulations, *Phys. Rev. E.*, **79**(046704), 1-14 (2009).

[7] D. Yu, R. Mei, L.S. Luo, and W. Shyy, Viscous flow computations with the method of lattice Boltzmann equation, Prog. Aerospace Sci., **39**, 329-367 (2003).

[8] J. Zhang, G. Yan, and X. Shi, Lattice Boltzmann model for wave propagation, *Phys. Rev. E.*, **80**(026706), 1-13 (2009).

[9] J.C.G. Verschaeve, Analysis of the lattice Boltzmann Bhatnagar-Gross-Krook no-slip boundary condition: Ways to improve accuracy and stability, *Phys. Rev. E.*, **80**(036703), 1-23 (2009).

[10] J. Boyd, J. Buick, J.A. Cosgrove, and P. Stansell, Application of the lattice Boltzmann model to simulated stenosis growth in a two-dimensional carotid artery, *Phys. Med. Biol.*, **50**, 4783-4796 (2005).

[11] M. Tamagawa, H. Kaneda, M. Hiramoto, and S. Nagahama, simulation of thrombus formation in shear flows using lattice Boltzmann method, *Artif. Organs*, **33**(8), 604-610 (2009).

[12] L. Axner, A.G. Hoekstra, A. Jeays, P. Lawford, R. Hose, and P.M.A. Sloot, Simulations of time harmonic blood flow in the Mesenteric artery: comparing finite element and lattice Boltzmann methods, *Biomed. Eng. Online*, **8**(23), 1-8 (2009).

[13] M. Krafczyk, M. Cerrolaza, M. Schulz, and E. Rank, Analysis of 3D transient blood flow passing through an artificial aortic valve by Lattice-Boltzmann methods, *J. Biomech.*, **31**, 453-462 (1998).

[14] I. Tanno, K. Morinishi, K. Matsuno, and H. Nishida, Validation of virtual flux method for forced convection flow, *JSME Int. J.*, **B49**(4), 1141-1148 (2006).

[15] P.L. Bhatnagar, E.P. Gross, and M. Krook, A model for collision processes in gases: I. Small amplitude processes in changed and neutral one-component system, *Phys. Rev.*, **94**, 511-525 (1954).

[16] J.D.Sterling and S. Chen, Stability analysis of lattice Boltzmann methods, *J. Comput. Phys.*, **123**, 196-206 (1996).

[17] Y.H. Quian, D. d'Humieres, and P. Lallemand, Lattice BGK models for Navier-Stokes equation, *Europhys. Lett.*, **17**, 479-484 (1992).

[18] X. He and L.S. Luo, Lattice Boltzmann model for the incompressible Navier-Stokes equation, *J. Stat. Phys.*, **88**, 927-944 (1997).